Journal of Translational Medicine

RESEARCH

Open Access

FlaA N/C attenuates radiation-induced lung injury by promoting NAIP/NLRC4/ASC inflammasome autophagy and inhibiting pyroptosis

Shihua Deng[1,2†], Yueyan Yang[1,2†], Shuang He[1,2†], Zixin Chen[1,2†], Xun Xia[1,2], Ting Zhang[1,2], Qing Yin[1,2], Teng Liu[1,2], Dongming Wu[1,2*], Kejian Pan[4*] and Ying Xu[1,2,3*]

Abstract

Background Radiation-induced lung injury (RILI) is the most common complication experienced by patients with thoracic tumors after radiotherapy. Among patients receiving thoracic tumor radiotherapy, 14.6–37.2% develop RILI. RILI is characterized by an acute inflammatory response; however, the exact mechanism remains unclear and an ideal drug is still lacking. In this study, we investigated the protective effects of flagellin A with linked C- and N-terminal ends (FlaA N/C) against the development of RILI.

Methods Mice and bronchial epithelial cells were exposed to radiation (15 Gy) after FlaA N/C treatment. Lung injury, bronchial epithelial cell injury, and RILI were assessed by histological evaluation in vivo and cell viability and cell death detection in vitro. Pyroptosis was assessed by western blotting (WB), immunofluorescence (IF), and immunohistochemistry (IHC). To explore the molecular mechanisms by which FlaA N/C inhibits RILI, conditional Beclin 1 (*Beclin1*$^{+/-}$) and NLR family CARD domain-containing protein 4 (*Nlrc4*)-knockout (*Nlrc4*$^{-/-}$) mice were generated. An autophagy inhibitor was used for in vitro cell assays, and pyroptosis indicators were detected. Data were analyzed using one-way analysis of variance.

Results FlaA N/C attenuated radiation-induced lung tissue damage, pro-inflammatory cytokine release, and pyroptosis in vivo and cell viability, cell death, and pyroptosis in vitro. Mechanistically, FlaA N/C activated the neuronal apoptosis inhibitory protein (NAIP)/NLRC4/apoptosis-associated speck-like protein containing a caspase recruitment domain (ASC) inflammasome, which was then degraded during Beclin 1-mediated autophagy. Deletion of the FlaA N/C D0 domain reversed the inhibitory effect of FlaA N/C on radiation-induced pyroptosis in vivo and in vitro. Similarly, *Nlrc4*-knockout in vivo or inhibition of autophagy in vitro eliminated the protective effects of FlaA N/C against radiation-induced pyroptosis.

†Shihua Deng, Yueyan Yang, Shuang He and Zixin Chen contributed equally to this study and are co-first authors.

*Correspondence:
Dongming Wu
harvey1989@126.com
Kejian Pan
pankejian2005@cmc.edu.cn
Ying Xu
yingxu825@126.com
Full list of author information is available at the end of the article

Conclusions These results indicate that FlaA N/C attenuates RILI by promoting NAIP/NLRC4/ASC inflammasome autophagy and inhibiting pyroptosis. This study provides a potential approach for RILI intervention.

Keywords Radiation-induced lung injury, Flagellin A N/C, Inflammasome autophagy, Beclin 1, Pyroptosis

Introduction

Thoracic radiotherapy serves as a key therapeutic approach for treating thoracic tumors [1, 2]. However, it also exerts secondary effects on healthy lung tissue. Radiation-induced lung injury (RILI) is one of the most common and serious radiation injuries in patients with thoracic tumors after radiotherapy [3]. RILI is divided into two stages: early radiation pneumonia and late irreversible pulmonary fibrosis [4]. Among patients receiving thoracic tumor radiotherapy, 14.6–37.2% develop RILI, which seriously limits treatment effects and affects patients' quality of life [5]. Currently, alternative, safe, and effective clinical treatment strategies and drug options are lacking. Therefore, the identification of effective drugs or methods to treat RILI during radiotherapy is vital. Several agents have been developed to protect against radiation exposure. Amifostine, approved by the Food and Drug Administration, has been used to protect patients with tumors receiving high-dose radiotherapy. However, owing to the limited route of administration, narrow protection window, and major adverse effects, the widespread use of this radiation-protection agent is limited [6, 7]. We previously synthesized a recombinant protein named flagellin A with linked C- and N-terminal ends (FlaA N/C) based on flagellin isolated from *Legionella pneumophila*, and found that FlaA N/C could attenuate radiation-induced intestinal injury and experimental autoimmune encephalomyelitis via pyroptosis inhibition [8, 9]. However, the role and mechanism of FlaA N/C in RILI remains unclear. Therefore, we hypothesized that FlaA N/C may act as a protective agent against RILI by inhibiting pyroptosis.

Ionizing radiation (IR) acts directly on tumor cells, damaging DNA and ionizing reactive oxygen species (ROS) within cells to cause indirect DNA damage, thereby achieving the goal of radiation therapy [10]. During radiation therapy, the radiation field inevitably includes healthy tissue. This may lead to increased ROS levels and DNA damage in normal cells. Studies have shown that ROS and DNA damage can induce NLR family pyrin domain containing (NLRP) 3 and apoptosis inhibitor of macrophage 2 (AIM2) inflammasome activation, mediating radiation-induced cell pyroptosis [11, 12]. Pyroptosis is a novel mode of inflammatory cell death that has only recently been discovered and confirmed [13]. During pyroptosis, the inflammasome complex is primarily composed of three components: pattern recognition receptors, adapter protein ASC, and caspase-1 precursor. Moreover, pyroptosis promotes the release of inflammatory factors and aggravates the inflammatory response [14]. Recent findings highlight the critical role of pyroptosis in RILI [15, 16]. For instance, Zhang et al. demonstrated that dsDNA-cGAS-STING-NLRP3 axis-mediated pyroptosis contributes to RILI [15]. Zhang et al. found that the NLRP3 inflammasome mediates pyroptosis of alveolar macrophages to induce RILI [16]. Therefore, the inhibition of pyroptosis is expected to be a novel and effective treatment for RILI.

Autophagy is a common protective homeostatic mechanism in cells. It is a cyclic process in which cells use enzymes in the lysosome to target and degrade necrotic organelles and biomacromolecules, thereby providing basic molecules for organelle renewal or cell metabolism [17]. Previous studies have shown that activating autophagy can effectively alleviate radiation-induced tissue damage, including damage to the lungs [18], skin [19], and brain [20], whereas inhibiting autophagy may potentially worsen radiation injury [21]. Studies have also shown that activation of inflammasome autophagy can significantly inhibit pyroptosis [22, 23]. Although the links between autophagy, pyroptosis, and RILI have not been fully examined, the activation of autophagy to inhibit pyroptosis is expected to become a new treatment strategy for RILI.

In this study, we established mouse and cell injury models of RILI and demonstrated that FlaA N/C protects against RILI and inhibits pyroptosis. Furthermore, we found that FlaA N/C activated the NAIP/NLRC4/ASC inflammasome via its D0 domain and mediated autophagy-dependent degradation. D0 domain deletion or inhibition of autophagy reversed FlaA N/C-induced inhibition of pyroptosis in vitro. In addition, conditional knockdown of *Beclin 1* and knockout of *Nlrc4* in mice were used to verify the effect of Beclin 1-mediated autophagy on FlaA N/C-induced pyroptosis inhibition. Collectively, our findings suggest that FlaA N/C is a promising therapeutic agent for RILI.

Methods

Antibodies and reagents

Primary antibodies anti-NLRP3 (ab263899), anti-NLRC4 (ab201792), anti-NAIP (ab129079), anti-ASC (ab155970), and anti-microtubule-associated protein 1A/1B-light chain 3 (LC3; ab243506) were purchased

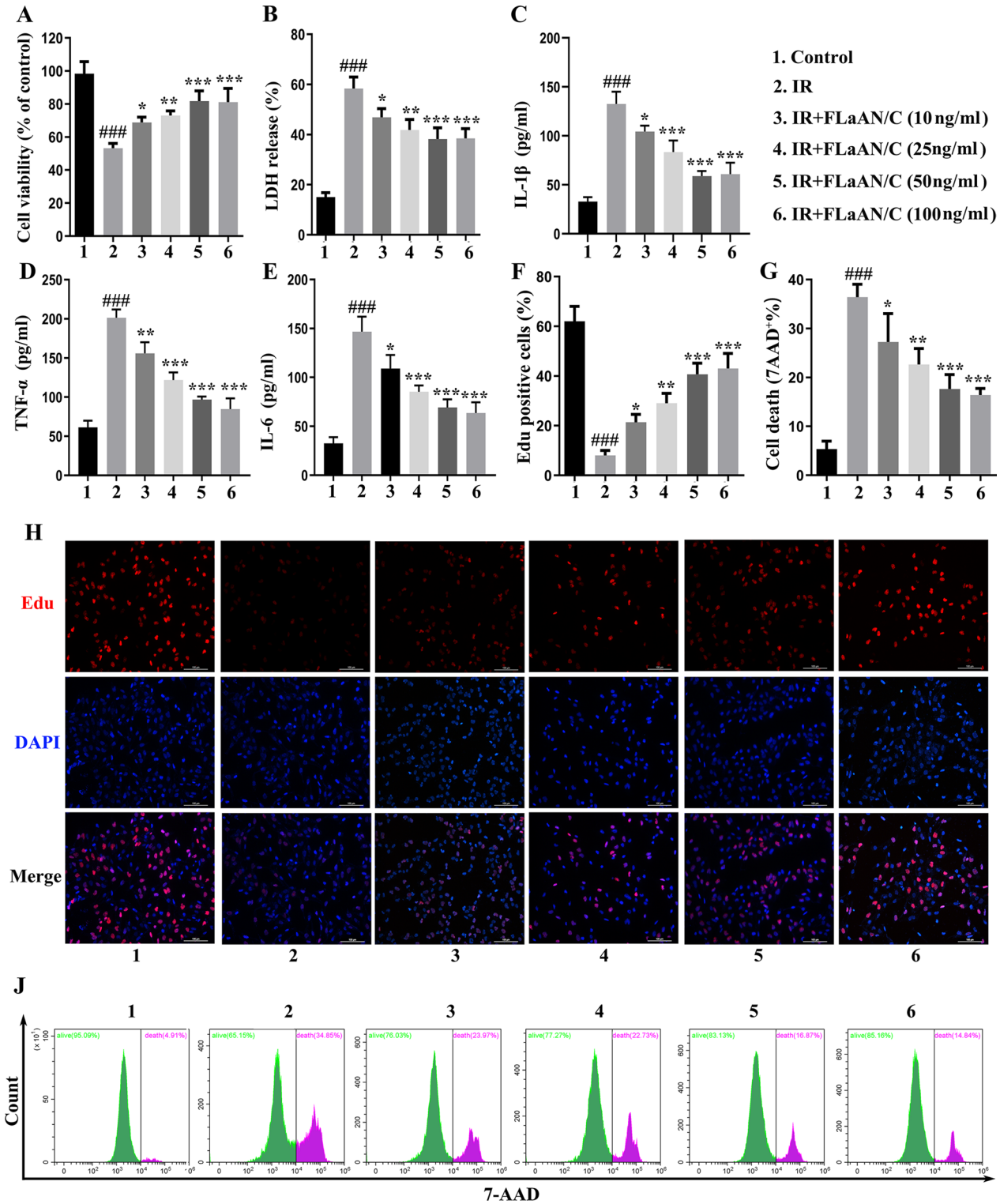

Fig. 1 Effects of FlaA N/C on radiation-induced lung epithelial cell injury. **a** BEAS-2B cell viability was determined using CCK-8 assay. **b** Lactate dehydrogenase (LDH) release. **c**–**e** Levels of IL-1β, TNF-α, and IL-6 in cell supernatants. **f, h** Cell proliferation was evaluated using the EDU assay. **g, j** 7AAD staining showing cell death. All experiments were repeated three times, and the data are shown as the mean ± SD. $^{\#}$ vs. control group, $^{\#\#\#}$ $P < 0.001$; * vs. IR group, *, **, and *** indicate $P < 0.05$, $P < 0.01$, and $P < 0.001$, respectively

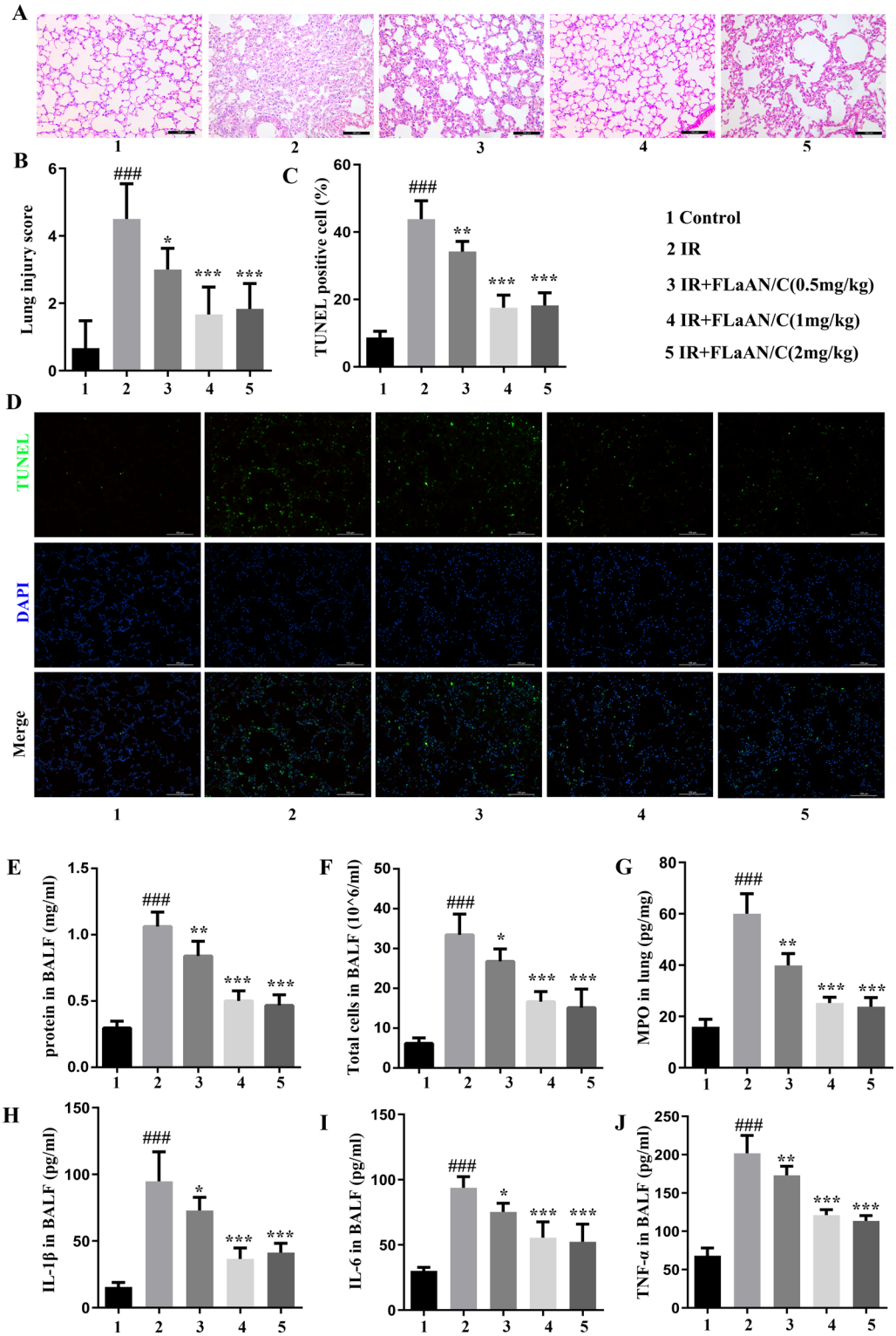

Fig. 2 Protective effects of FlaA N/C against RILI in mice. **a** Representative hematoxylin and eosin (H&E)-stained lung tissue images (scale bars = 100 μm). **b** Lung injury score. **c** TUNEL-positive cell rate. **d** Representative TUNEL-stained lung tissue images (scale bars = 100 μm). **e**, **f** Total protein concentrations and cell count in BALF. **g** MPO activity in lung tissues. **h**–**j** Levels of IL-1β, IL-6, and TNF-α in BALF. The data are shown as the mean ± SD. $^{\#}$ vs. control group, $^{\#\#\#}$ $P < 0.001$; * vs. IR group, *, **, and *** indicate $P < 0.05$, $P < 0.01$, and $P < 0.001$, respectively

from Abcam. Anti-gasdermin D (GSDMD; #39754) and anti-GSDMD-N (#36425) antibodies were obtained from Cell Signaling Technology. Anti-caspase 1 p20 (PA5-99390) and anti-interleukin (IL)-1β (PA5-105048) antibodies were obtained from Thermo Fisher Scientific. Anti-IL-18 (10663-1-AP), anti-Beclin 1 (11306-1-AP), anti-LC3 (81004-1-RR), AIM2 (66902-1-Ig), His-Tag (66005-1-Ig), anti-GAPDH (60004-1-Ig), and horseradish peroxidase-conjugated goat anti-mouse (SA00001-1) and rabbit anti-goat (SA00001-2) secondary antibodies were obtained from Proteintech (Wuhan, China). FLaAN/C and D0 domain deletion FLaAN/C (ΔFLaAN/C) recombinant proteins were generated by Beijing Protein Innovation Co., Ltd. (Beijing, China). The autophagy inhibitor, 3-methyladenine (3-MA), was obtained from Selleck Chemicals.

Animals and thoracic radiation

Male C57BL/6 mice (8–10 weeks old) were purchased from GemPharmatech (Chengdu, China). Lung-specific *Nlrc4*-knockout (KO) transgenic ($Nlrc4^{-/-}$) and Beclin1 haploinsufficiency ($Beclin1^{+/-}$) mice were generated by Beijing Viewsolid Biotech Co., Ltd. All mice were maintained in cages with free access to food and water at 24 ± 2 °C under 40–70% relative humidity with a 12:12-h light/dark cycle. All animal experiments were approved by The Animal Policy and Welfare Committee of Chengdu Medical College (Approval No: CMC-IACUC-2021024). For thoracic IR, mice were placed horizontally after intraperitoneal injection of pentobarbital sodium (50 mg/kg), and the other parts outside the chest were covered with lead plates. The lungs of each mouse were irradiated with a single 15-Gy X-ray dose according to previous research [24, 25] using an X-RAD 160–225 instrument (Precision X Ray Inc., Branford, CT, USA; filter: 2 mm, AI; 42 cm, 225 kv/s, 12.4 mA, and 2.0 Gy/min).

Mice were randomly divided into five groups (n = 6 mice/group) for lung injury detection: control, IR (each mouse received 15-Gy radiation), and IR + FlaA N/C (0.5, 1, or 2 mg/kg). For the loss-of-function study, wild-type (WT) and $Nlrc4^{-/-}$ (or $Beclin1^{+/-}$) mice were randomly divided into six groups (n = 6 mice/group): WT, $Nlrc4^{-/-}$ (or $Beclin1^{+/-}$), WT + IR, $Nlrc4^{-/-}$ (or $Beclin1^{+/-}$) + IR, WT + IR + FlaA N/C (1 mg/kg), and $Nlrc4^{-/-}$ (or $Beclin1^{+/-}$) + IR + FlaA N/C (1 mg/kg). Fourteen days after irradiation, the mice were euthanized via intraperitoneal injection of sodium pentobarbital (120 mg/kg), and their lungs and bronchoalveolar lavage fluid (BALF) were collected.

Cell culture and transfections

Bronchial epithelial BEAS-2B cells were obtained from the Cell Bank of the Chinese Academy of Sciences (Shanghai, China). The cells were cultured in RPMI-1640 medium containing 10% fetal bovine serum and 5 mg/mL penicillin/streptomycin at 37 °C under 5% CO_2. NLRC4 silencing lentivirus shNLRC4 (5′-GGATGAACG TGC TAGAACA-3′) and negative control lentiviral shNC (5′-TTCTCCGAAC GTGTCACGT-3′) were obtained from Genomeditech (Shanghai, China), and cell transfection was performed according to the manufacturer's instructions.

Radiation-induced cell injury models

BEAS-2B cells were cultured in a 10-cm plate for 24 h and divided into control (Con) and IR groups according to experimental requirements. The IR group received 15 Gy of X-rays. The supernatant was collected and the cytokine concentration was measured 24 h after irradiation. Cells were collected for subsequent experiments.

Cell Counting Kit-8 assay and lactate dehydrogenase release assay

Cell Counting Kit-8 (CCK-8; Beyotime, C0043) and lactate dehydrogenase (LDH; Beyotime, C0017) release assays were performed to measure cell injury according to the manufacturer's instructions [26].

Enzyme-linked immunosorbent assay

The concentrations of IL-6, tumor necrosis factor (TNF)-α, IL-18, and IL-1β in BALF, mouse serum, and cell culture supernatants were determined using commercial enzyme-linked immunosorbent assay (ELISA)

(See figure on next page.)

Fig. 3 FlaA N/C inhibits pyroptosis in a radiation-induced lung epithelial cell injury model. **a** CCK-8 assay was used to determine changes in BEAS-2B cell viability. **b** Level of LDH release. **c** Viability of caspase-1 in cell supernatants. **d**, **e** Levels of IL-1β and IL-18 in cell supernatants determined using ELISA. **f**, **g** 7AAD staining showing cell death. **h** WB was used to detect the protein expression of IL-1β, IL-18, Caspase-1 p20, and GSDMD-N in BEAS-2B cells. **i**, **j** Representative IF images and quantification of fluorescence intensity of GSDMD-N in BEAS-2B cells (scale bars = 20 μm). All experiments were repeated three times, and the data are shown as the mean ± SD. $^{\#}$ vs. control group, $^{\#\#\#}$ $P < 0.001$; * vs. IR group, *, **, and *** indicate $P < 0.05$, $P < 0.01$, and $P < 0.001$, respectively

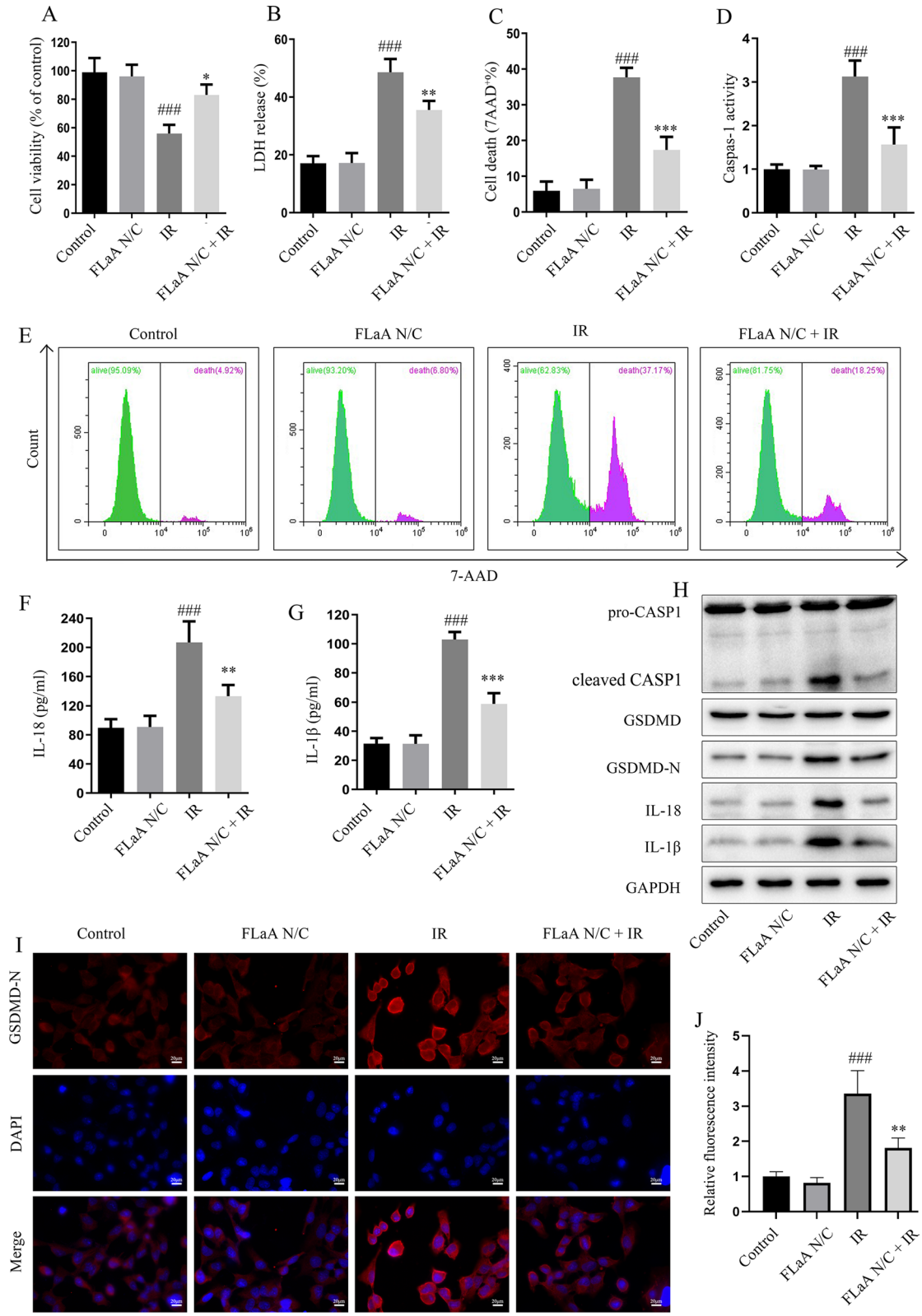

Fig. 3 (See legend on previous page.)

kits (Mlbio, Shanghai, China) according to the manufacturer's instructions.

Histopathologic analysis

Hematoxylin and eosin (H&E) staining was performed as previously described [26]. Lung sections were stained with H&E (G1120; Solarbio, Beijing, China), and all images were captured using a DM4000 microscope (LEICA, Wetzlar, Germany) equipped with 20× and 40× objective lenses (LEICA) and a DFC450 C camera (LEICA). The degree of lung injury was scored using a five-point scoring system (0–4) by measuring neutrophil infiltration, edema, disorganization of the lung parenchyma, and hemorrhage [27]. Up to four categories were added to obtain the total lung injury score (maximum score, 16).

Western blotting, immunofluorescence, and immunohistochemical analysis

Western blotting (WB), immunofluorescence (IF), and immunohistochemical (IHC) assays were performed, as previously described, to measure the expression of pyroptosis-related proteins [26]. All primary antibodies were used at a 1:1000 dilution for WB and 1:100 for IF and IHC.

Cell death assay

Cells were collected, washed twice with phosphate-buffered saline (PBS), and stained using a 7-AAD detection kit (Beyotime, Shanghai, China) according to the manufacturer's instructions. The cells were then analyzed using a flow cytometer (FACSCalibur; Becton, Dickinson and Company), and the data were processed using CytExpert software (Beckman Coulter, Inc.).

5′-Ethynyl-2′-deoxyuridine assay

The 5′-ethynyl-2′-deoxyuridine (EdU) assay was performed as previously described [26]. Briefly, BEAS-2B cells were seeded in 24-well plates and incubated with EdU working solution (Beyotime) at 37 °C for 30 min. After washing thrice with PBS, DAPI (1:5 000) was added to the samples, which were then incubated at 37 °C for 5 min in the dark. Images were randomly captured at 200× magnification using a fluorescence microscope (Leica Microsystems Inc.).

Transmission electron microscopy

Autophagy of BEAS-2B cells and lung tissue cells was analyzed via transmission electron microscopy (TEM; FEIG2; Thermo Fisher Scientific, Inc.) as previously described [26]. Briefly, the cells or lung tissues were fixed in 2.5% glutaraldehyde and then incubated in 0.1 M osmium tetroxide for 2 h or longer at 25 °C. After further dehydration, permeation, and embedding, 65 nm ultrathin sections were obtained and viewed using TEM.

Real-time fluorescent quantitative polymerase chain reaction

Real-time fluorescent quantitative polymerase chain reaction (RT-qPCR) was performed as previously described [26]. The sense and antisense primer sequences for *NLRC4* were as follows: forward, 5′-GATGTGTCC AGCGTGAATGAGG-3′; reverse, 5′-GAGAAGGCA GCCGTGTTGATAC-3′. The sense and antisense primer sequences for *ASC* were as follows: forward, 5′-GTCAGC TTCTAACTGGAGACCTAC-3′ and reverse, 5′-GAC CTTCCCGTACAGAGCATCC-3′. *GAPDH* was used as an internal control. The sense and antisense primer sequences for *GAPDH* were as follows: forward, 5′-CAG GAGGCATTGCTGATGAT-3′; reverse, 5′-GAAGGC TGGGGCTCATTT-3′. The relative expression levels were calculated using the $2^{-\Delta\Delta CT}$ method.

Statistical analysis

All in vitro experiments were performed independently at least thrice, and all animals were randomly assigned to the experimental groups. Data are presented as the mean ± standard deviation and were analyzed using GraphPad Prism 7 software (GraphPad Software; Dotmatics). Significance was determined using one-way analysis of variance (ANOVA), followed by Tukey's post-hoc test. Statistical significance was set at $P < 0.05$.

(See figure on next page.)

Fig. 4 FlaA N/C activates the NAIP/NLRC4/ASC inflammasome and induces autophagy. **a** Western blotting (WB) results showing the effect of FlaA N/C on NLRP3, AIM2, NLRC4, and ASC protein levels. **b** WB results showing the effect of FlaA N/C on ASC and NLRC4 expression. **c** WB results showing the effect of radiation on the expression of caspase-1 p20 and GSDMD-N. **d** *ASC* and *NLRC4* mRNA expression levels were assayed using qRT-PCR. **e** The effect of FlaA N/C on the activation of NAIP/NLRC4/ASC was determined using Co-IP. **f** WB results showing the effect of FlaA N/C on the expression of LC3. **g** TEM was used to determine the effect of FlaA N/C on autophagosome formation (scale bars = 1 μm). **h** Autophagy of the NAIP/NLRC4/ASC inflammasome was detected using fluorescence colocalization (scale bars = 5 μm)

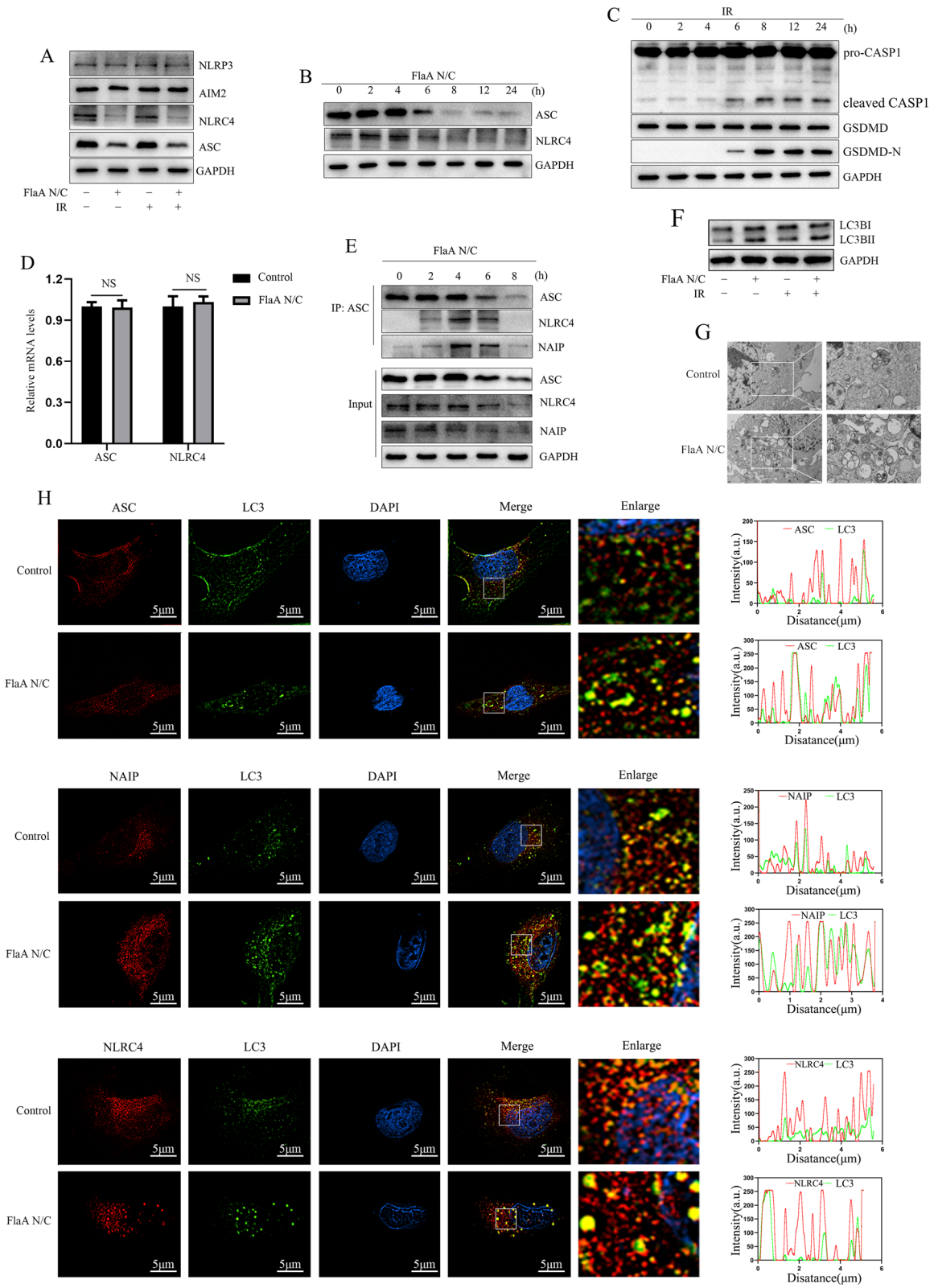

Fig. 4 (See legend on previous page.)

Results

FlaA N/C protected against radiation-induced bronchial epithelial cell injury

To explore the role of FlaA N/C in radiation-induced bronchial epithelial cell injury in vitro, a radiation-induced cell injury model was established after FlaA N/C pretreatment for 2 h. As expected, the radiation-induced inhibition of cell activity (Fig. 1a) and proliferation (Fig. 1f, h), LDH release (Fig. 1b), secretion of inflammatory cytokines (Fig. 1c–e), and increased cell death (Fig. 1g, j) were abrogated by FlaA N/C pretreatment in a dose-dependent manner. The results also indicated that 50 and 100 ng/mL FlaA N/C had similar protective effects on cell viability and LDH release from BEAS-2B cells. Therefore, 50 ng/mL FlaA N/C was selected for subsequent cell experiments. These results suggested that FlaA N/C protects against radiation-induced bronchial epithelial cell injury.

FlaA N/C attenuated RILI in a mouse model

The role of FlaA N/C in RILI in vivo was investigated in an RILI mouse model. FlaA N/C markedly decreased morphological changes and cell death in irradiated mice in a dose-dependent manner, as determined using H&E (Fig. 2a and b) and TUNEL (Fig. 2c and d) staining, respectively. Furthermore, the protein concentrations and total cell counts in the BALF increased significantly after exposure to radiation compared with those in the control group (Fig. 2e and f). FlaA N/C markedly decreased protein leakage and the total number of cells in the BALF. Moreover, FlaA N/C decreased myeloperoxidase activity in mouse lung tissue compared with that in the IR-only group (Fig. 2g) and effectively reduced IL-1β, IL-6, and TNF-α levels in the BALF (Fig. 2h–j). Overall, these results indicate that FlaA N/C protected mice against RILI. In addition, our results indicate that 1 and 2 mg/kg FlaA N/C had similar protective effects against RILI. We determined the biosafety of FlaA N/C (1 mg/kg); FlaA N/C treatment (1 mg/kg) exhibited minimal toxicity in vivo ((supplementary Fig. 1). Based on these findings, 1 mg/kg FlaA N/C was selected for the subsequent mouse experiments.

FlaA N/C attenuated RILI by inhibiting pyroptosis

Pyroptosis is a major mechanism responsible for RILI [16]. We have previously shown that FlaA N/C attenuates radiation-induced intestinal injury by inhibiting pyroptosis. In this study, pyroptosis parameters were evaluated in vivo and in vitro to investigate whether FlaA N/C inhibits pyroptosis in RILI. Consistent with our previous findings, the present results showed that FlaA N/C significantly inhibited radiation-induced decreases in BEAS-2B cell activity (Fig. 3a), LDH release (Fig. 3b), and cell death (Fig. 3f and g). In the mouse model, the intense morphological changes observed via H&E staining were significantly reduced by FlaA N/C (supplementary Fig. 2a). Moreover, the significant increase in caspase-1 activity in BEAS-2B cells after irradiation was attenuated by FlaA N/C pretreatment (Fig. 3c). Consistent with the changes in caspase-1 activity, FlaA N/C significantly inhibited the radiation-induced secretion of IL-1β and IL-18 in vivo ((supplementary Fig. 2d and e) and in vitro (Fig. 3d and e). Furthermore, the increased protein levels of caspase-1 p20, IL-1β, IL-18, and GSDMD-N, as quantified using WB, IF, and IHC, were suppressed by FlaA N/C pretreatment (supplementary Fig. 2b and c; Fig. 3h and i). These results indicate that FlaA N/C alleviates RILI by inhibiting pyroptosis.

FlaA N/C activated the NAIP/NLRC4/ASC inflammasome and induced autophagy

Previous studies have shown that NLRP3 and AIM2 inflammasomes, rather than NLRC4 inflammasomes, mediate radiation-induced pyroptosis. We validated this conclusion further (supplementary Fig. 3). To investigate the mechanism by which FlaA N/C inhibits pyroptosis, we examined the effects of FlaA N/C on the expression of NLRP3, AIM2, NLRC4, and ASC proteins. FlaA N/C significantly reduced NLRC4 and ASC expression, but had no effect on NLRP3 and AIM2 expression; however, this finding may not be

(See figure on next page.)

Fig. 5 FlaA N/C activates the NAIP/NLRC4 inflammasome through its D0 domain and mediates autophagy by competitive binding with NLRC4 and Beclin1. **a** Domains and similar secondary structural regions of Beclin1 and NAIP. **b**, **c** Predicted binding model for NLRC4 and Beclin-1. **b** Surface bonding model of NLRC4 and Beclin-1. **c** 3D combined model of NLRC4 and Beclin-1. The backbone of NLRC4 is shown in pink and that of Beclin-1 is indicated in green. **d**, **e** Predicted binding models for NLRC4 and NAIP. **d** Surface binding model of NLRC4 and NAIP. **e** 3D combined model of NLRC4 and NAIP. The backbone of NAIP is shown in blue. **f**–**g** Co-IP assay was used to detect the (**f**) binding of Beclin-1 and NLRC4 and (**g**) binding of FlaA N/C and Δ FlaA N/C with NLRC4. **h** Autophagosome and autolysosome numbers in each group were calculated. **i** Confocal microscopy observation of mRFP-GFP-LC3 adenovirus-transfected BEAS-2B cells treated as indicated (scale bars = 10 μm). **j** TEM was used to determine the effects of ΔFlaA N/C on autophagosome formation (scale bars = 1 μm)

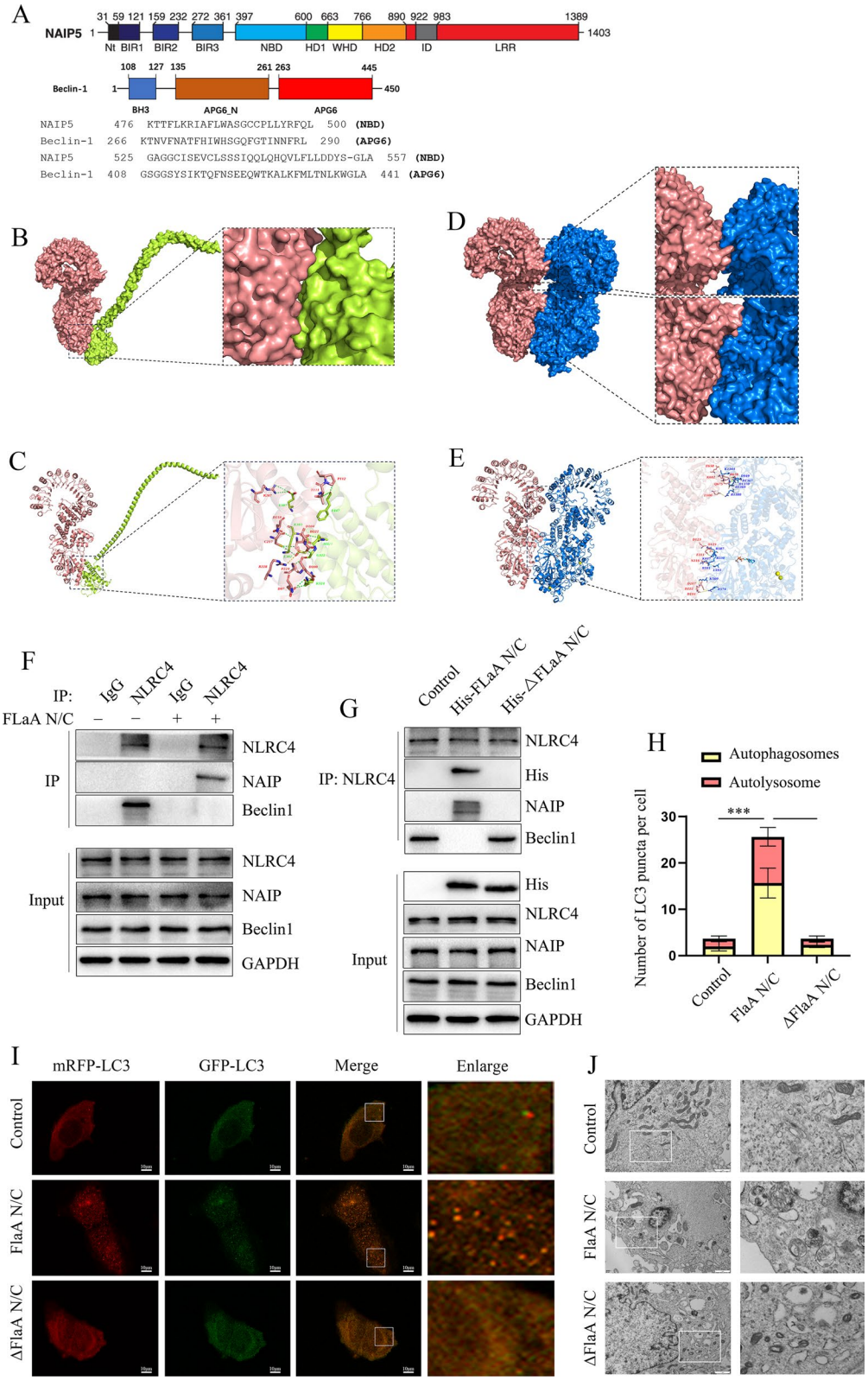

Fig. 5 (See legend on previous page.)

related to radiation (Fig. 4a). The effects of FlaA N/C on ASC and NLRC4 expression were examined at various time points. Our results show that the expression of both proteins was significantly inhibited after incubation with FlaA N/C for 8 h (Fig. 4b). The pyroptosis activation time after irradiation was also determined. There was obvious pyroptosis after 6 h of irradiation, which peaked at 8 h (Fig. 4c). Notably, FlaA N/C treatment had no effect on *NLRC4* and *ASC* mRNA levels (Fig. 4d). Thus, we hypothesized that FlaA N/C reduces ASC and NLRC4 protein expression through post-translational modifications, thereby hindering the activation of ASC-dependent NLRP3 and AIM2 inflammasomes and inhibiting pyroptosis, ultimately alleviating RILI.

FlaA N/C has a structure similar to that of flagellin and may activate the NAIP/NLRC4/ASC inflammasome instead of inhibiting protein expression. However, further investigation is required. NAIP/NLRC4/ASC inflammasomes were activated after 4 h of FlaA N/C treatment. After 6 h, this activation gradually reduced the expression of NLRC4 and ASC (Fig. 4e). Furthermore, we examined the role of FlaA N/C in activating the NAIP/NLRC4/ASC inflammasome following NLRC4 silencing. We confirmed that NLRC4 silencing reversed the interaction and colocalization of NAIP and ASC (supplementary Fig. 4). In recent years, autophagy, an important post-translational regulatory mechanism of proteins, has been extensively studied for its role in the maintenance of pyroptosis homeostasis. We hypothesized that FlaA N/C promotes the formation of NAIP/NLRC4/ASC inflammasomes accompanied by autophagy activation, thereby degrading NAIP/NLRC4/ASC. Six hours after the addition of FlaA N/C, the proportion of LC3II significantly increased and was independent of radiation (Fig. 4f). Electron microscopy revealed that FlaA N/C significantly induced autophagy (Fig. 4g). Fluorescence confocal microscopy showed that LC3 and NAIP/NLRC4/ASC inflammasomes were significantly colocalized (Fig. 4h). These findings indicated that FlaA N/C induces NAIP/NLRC4/ASC inflammasome autophagy.

FlaA N/C activated the NAIP/NLRC4 inflammasome via its D0 domain and mediated autophagy via the competitive binding of NLRC4 with Beclin 1

Further structural biological analysis showed that the autophagy-related protein Beclin 1 had a secondary structure similar to that of NAIP, and that both could bind to NLRC4 (Fig. 5a–e). Western blot analysis showed that Beclin 1 and NLRC4 existed in a complex under resting conditions, and the binding of NLRC4 and Beclin 1 was significantly weakened after FlaA N/C treatment (Fig. 5f). Flagellin recognizes its intracellular receptor, NAIP, via the D0 domain and forms the NAIP/NLRC4 inflammasome [28]. Considering that FlaA N/C contains the full-length D0 domain of flagellin, we hypothesized that FlaA N/C activates NAIP/NLRC4 via the D0 domain. Hence, we constructed FlaA N/C with a deletion mutation in the D0 domain (ΔFlaA N/C) and found that compared to FlaA N/C, ΔFlaA N/C could not competitively bind to NLRC4 (Fig. 5g). Autophagy flux analysis showed that the numbers of autophagosomes and autophagolysosomes increased after FlaA N/C treatment, whereas ΔFlaA N/C treatment resulted in a significant decrease (Fig. 5h–J). These results show that FlaA N/C activates the NAIP/NLRC4 inflammasome through its D0 domain, and that Beclin 1 dissociates and activates autophagy.

D0 domain deletion reversed the inhibitory effect of FlaA N/C on pyroptosis

After confirming that the D0 domain of FlaA N/C is essential for activation of the NAIP/NLRC4/ASC inflammasome, we further verified the function of ΔFlaA N/C. FlaA N/C significantly inhibited radiation-induced cell death and LDH release in BEAS-2B cells, whereas the opposite effect was observed with ΔFlaA N/C (Fig. 6a–c). Moreover, we validated that ΔFlaA N/C had no effect on radiation-induced caspase-1 and GSDMD activation and IL-1β and IL-18 secretion in vivo (supplementary Fig. 5a–d) and in vitro (Fig. 6d–f, h and i). These results were confirmed using in vivo (supplementary Fig. 5e) and in vitro (Fig. 6g) WB analyses.

(See figure on next page.)

Fig. 6 D0 domain deletion reverses the inhibitory effect of FlaA N/C on pyroptosis in vitro. **a**, **b** 7AAD staining showing BEAS-2B cell death. **c** Level of LDH release. **d** Viability of caspase-1 in cell supernatants. **e**, **f** Levels of IL-1β and IL-18 in cell supernatants determined using ELISA. **g** WB was used to detect IL-1β, IL-18, caspase-1 p20, and GSDMD-N protein expression in BEAS-2B cells. **h**, **i** Quantification of fluorescence intensity and Representative IF images of GSDMD-N in BEAS-2B cells (scale bars = 20 μm). All experiments were repeated three times, and the data are shown as the mean ± SD. $^{\#}$ vs. control group, $^{\#}$, $^{\#\#}$, and $^{\#\#\#}$ indicate $P < 0.05$, $P < 0.01$, and $P < 0.001$, respectively; * vs. FlaA N/C + IR group. *, **, and *** indicate $P < 0.05$, $P < 0.01$, and $P < 0.001$, respectively

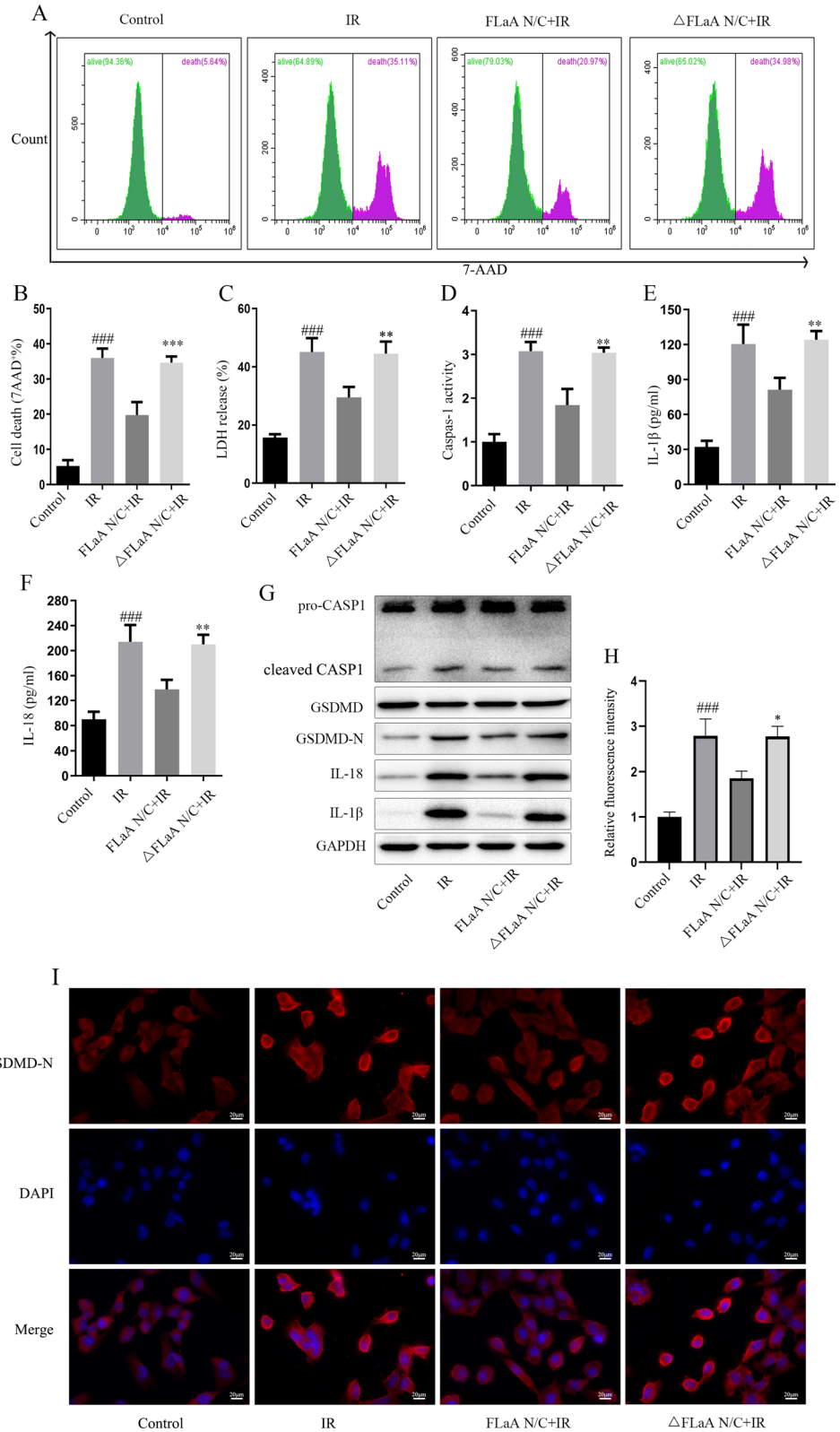

Fig. 6 (See legend on previous page.)

Beclin1 knockdown reversed FlaA N/C-induced inhibition of pyroptosis

To verify the role of Beclin 1 in the FlaA N/C-mediated inhibition of radiation-induced pyroptosis, *Beclin1*$^{+/-}$ mice were generated. *Beclin1* knockdown was confirmed using WB (Fig. 7f). Notably, *Beclin1* knockdown significantly reversed FlaA N/C-mediated protection against morphological changes (Fig. 7a and c). Similarly, known pyroptosis events, including caspase-1, GSDMD, IL-1β, and IL-18 activation (Fig. 7b and d–f), occurred to a greater extent in *Beclin1*$^{+/-}$ + IR + FlaA N/C mice than in WT + IR + FlaA N/C mice. Autophagy was detected after *Beclin1* knockdown, which significantly attenuated FlaA N/C-induced autophagy (Fig. 7f and g). These results indicate that Beclin 1-mediated autophagy is essential for FlaA N/C-induced inhibition of pyroptosis.

Inhibition of autophagy reversed FlaA N/C-induced inhibition of pyroptosis in vitro

The autophagy inhibitor 3-mA was used in a multiplex assay to verify that autophagy is essential for the FlaA N/C-induced inhibition of pyroptosis. The results consistently showed that inhibition of autophagy by 3-mA significantly reduced the radioprotective and pyroptosis-inhibitory effects of FlaA N/C, as determined by cell death (Fig. 8a and b), LDH release assay (Fig. 8c), and caspase-1, GSDMD, IL-1β, and IL-18 activation assays (Fig. 8d–g). In addition, WB and TEM were used to measure the expression of the autophagy marker LC3 and autophagosome formation in each group (Fig. 8g and h). Compared with the IR group, autophagy in the FlaA N/C + IR group was elevated, but was repressed in the FlaA N/C + IR + 3-MA group. These results further indicated that FlaA N/C promotes autophagy and inhibits radiation-induced pyroptosis in BEAS-2B cells.

Nlrc4 KO reversed FlaA N/C-induced inhibition of pyroptosis

The results showed that FlaA N/C could clear ASCs by promoting the formation of NAIP/NLRC4/ASC inflammasomes and autophagy, thereby inhibiting radiation-induced pyroptosis. This observation was further verified using *Nlrc4*$^{-/-}$ mice to disrupt FlaA N/C-induced formation of the NAIP/NLRC4/ASC inflammasome and inhibit autophagy. H&E staining was performed to measure morphological changes in each group. *Nlrc4* KO significantly reversed FlaA N/C-mediated protection against morphological changes (Fig. 9a and c). IHC, WB, and ELISA were performed to determine the expression of pyroptosis markers in each group (Fig. 9b and d–g). The results showed that pyroptosis marker levels were lower in the WT + IR + FlaA N/C group than in the WT + IR group. However, *Nlrc4* KO had an inverse effect on pyroptosis, as observed in the *Nlrc4*$^{-/}$ + IR + FlaA N/C group. These results indicate that *Nlrc4* KO reverses the FlaA N/C-mediated inhibition of radiation-induced pyroptosis.

Discussion

This study showed that FlaA N/C ameliorated RILI both in vivo and in vitro and concomitantly inhibited pyroptosis. Initially, we observed that FlaA N/C reduced the radiation-induced inflammatory response and cell/lung injury. Our results clearly show that FlaA N/C significantly inhibited radiation-induced pyroptosis. FlaA N/C also selectively promoted the formation of the NAIP/NLRC4/ASC inflammasome and its degradation via activation of Beclin 1-mediated autophagy. Furthermore, *Nlrc4* KO or inhibition of autophagy abolished the FlaA N/C-induced inhibition of pyroptosis and its protective effects against RILI. Collectively, these results indicate that FlaA N/C is a promising pharmacological agent that can be used to prevent RILI.

Radiation-induced excessive release of pro-inflammatory cytokines is the primary cause of tissue damage [29]. The mechanisms underlying radiation-induced inflammatory cytokines have not been fully elucidated. Pyroptosis is a novel mode of inflammatory cell death that is accompanied by the production of large amounts of inflammatory cytokines [13]. Previous studies have shown that pyroptosis is involved in radiation-induced lung [15, 16, 25], brain [30], and skin [31] injury. We previously demonstrated the involvement of pyroptosis in radiation-induced intestinal injury [8]. Consistent with previous findings, this study demonstrated that pyroptosis was involved in RILI. Therefore, targeting pyroptosis may protect against RILI.

(See figure on next page.)

Fig. 7 *Beclin1* knockdown reverses FlaA N/C-induced inhibition of pyroptosis. **a** Representative hematoxylin and eosin (H&E)-stained mouse lung tissue images (scale bars = 100 μm). **b** Representative images of mouse lung tissues stained for GSDMD-N using immunohistochemistry (scale bars = 50 μm). **c** Lung injury score. **d**, **e** Serum Levels of IL-1β and IL-18. **f** Expression of IL-1β, IL-18, caspase-1 p20, GSDMD-N, and LC3 in lung tissues was detected using WB. **g** TEM was used to determine the effects of *Beclin1* knockdown on FlaA N/C-induced autophagosome formation in mouse lung tissues (scale bars = 2 μm). The data are shown as the mean ± SD. $^{\#}$ vs. WT group, $^{\#}$, $^{\#\#}$, and $^{\#\#\#}$ indicate $P < 0.05$, $P < 0.01$, and $P < 0.001$, respectively; * vs. WT + IR + FlaA N/C group. *, **, and *** indicate $P < 0.05$, $P < 0.01$, and $P < 0.001$, respectively

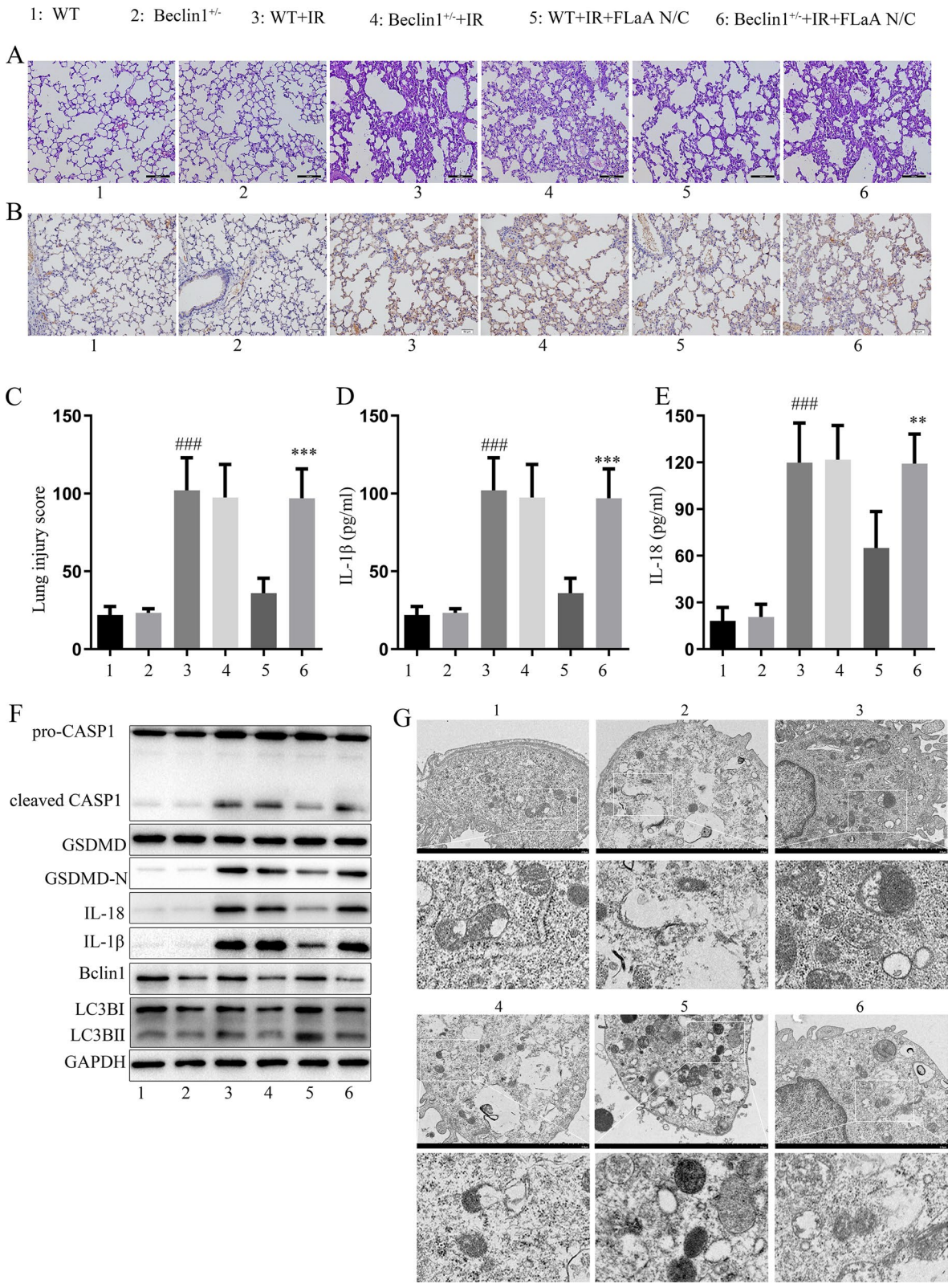

Fig. 7 (See legend on previous page.)

Radiation-induced pyroptosis is primarily associated with NLRP3 and AIM2 inflammasomes [10, 32]. In this study, we found that radiation activated NLRP3 and AIM2 inflammasome-mediated pyroptosis in lung epithelial cells, whereas FlaA N/C significantly inhibited pyroptosis and RILI. Importantly, we found that monotreatment with FlaA N/C activated NAIP/NLRC4/ASC inflammasomes and subsequently induced their degradation. ASC is essential for NLRP3 and AIM2 inflammasomes to recruit caspase-1 and activate pyroptosis. Following degradation of the NAIP/NLRC4/ASC inflammasome, ASC is consumed, blocking NLRP3 and AIM2 inflammasome-mediated pyroptosis signaling pathways. In recent years, autophagy has been extensively studied in relation to the regulation of inflammasome activation [33]. Sun et al. showed that autophagy maintains normal energy levels and metabolism and reduces inflammation by limiting the direct release of pro-inflammatory cytokines by eliminating damaged mitochondria and activated inflammasomes [34]. Di et al. found that autophagy plays an important role in mediating inflammasome homeostasis [35]. A recent study highlighted that NLRC4 interacts with Beclin 1 to inhibit autophagosome maturation. When flagellin stimulates cells, NLRC4 and NAIP form a NAIP/NLRC4 complex, thereby reducing the inhibition of NLRC4 on Beclin 1 and inducing autophagy [36]. However, whether FlaA N/C induces NAIP/NLRC4/ASC inflammasome degradation by inducing autophagy and its potential mechanism is unclear.

Therefore, we examined the activation effect and mechanism of action of FlaA N/C on autophagy. It is well documented that LC3 is a hallmark molecule in autophagy research and that the number of autophagosomes can effectively indicate autophagy [37]. First, electron microscopy and fluorescence confocal microscopy revealed that FlaA N/C significantly increased the number of autophagosomes in BEAS-2B cells. Fluorescence confocal microscopy showed that FlaA N/C promoted LC3 and NAIP/NLRC4/ASC inflammasome colocalization in BEAS-2B cells. Second, the autophagy inhibitor 3-MA was used for cell analysis, and the results showed that inhibition of autophagy by 3-MA reversed FlaA N/C-induced inhibition of pyroptosis in vitro. To clarify the radiation-protective effect of FlaA N/C via NAIP/NLRC4/ASC inflammasome autophagy in vivo, *Beclin1*$^{+/-}$ and *Nlrc4*$^{-/-}$ mice were generated. The results showed that *Beclin1*-knockdown and *Nlrc4*-KO reversed FlaA N/C-induced autophagy and pyroptosis inhibition. Considering the importance of the D0 domain in flagellin, we examined its role by constructing ΔFlaA N/C. and found that the deletion of the D0 domain reversed the inhibitory effect of FlaA N/C on autophagy and pyroptosis. Overall, these results confirmed that FlaA N/C-induced NAIP/NLRC4/ASC activation relieved the inhibitory effect of NLRC4 on Beclin 1, induced inflammasome autophagy, and ultimately inhibited radiation-induced pyroptosis.

This study had certain limitations. First, further investigation is required to determine whether FlaA N/C influences other programmed cell death mechanisms such as ferroptosis. Second, there may be other mechanisms by which FlaA N/C regulates pyroptosis that must be assessed. Third, RILI typically consists of two phases: early radiation pneumonia and late pulmonary fibrosis. However, our study focused only on the first phase. Finally, the occurrence of radiation-induced pyroptosis in clinical RILI samples was not verified. To address the limitations of our study, our future research will first focus on investigating the regulatory effects of FlaA N/C on other cell death pathways in the context of a radiation-induced pulmonary fibrosis model and explore the underlying mechanisms. In addition, we will actively collaborate with clinicians to collect clinical samples of RILI and assess the feasibility of conducting clinical trials.

Conclusions

In this study, we used a combination of in vitro and animal models to demonstrate that FlaA N/C exerted significant protective effects against RILI. The mechanisms underlying these effects may involve inhibition of pyroptosis via the promotion of NAIP/NLRC4 inflammasome formation and autophagy (Fig. 10). These results elucidate a novel role of FlaA N/C as a safe and effective agent against RILI. Given the limitations of radioprotective agent options, this study may contribute to the development of novel radioprotective strategies for clinical

(See figure on next page.)

Fig. 8 Autophagy inhibition reverses the inhibitory effect of FlaA N/C on pyroptosis in vitro. **a**, **b** 7AAD staining showing BEAS-2B cell death. **c** Level of LDH release. **d**, **e** Levels of IL-1β and IL-18 in cell supernatants detected using ELISA. **f** Viability of caspase-1 in cell supernatants. **g** WB was used to detect IL-1β, IL-18, caspase-1 p20, GSDMD-N, and LC3 protein expression in BEAS-2B cells. **h** TEM was used to determine the effect of 3-MA on FlaA N/C-induced autophagosome formation in BEAS-2B cells (scale bars = 1 μm). All experiments were repeated three times, and the data are shown as the mean ± SD. $^{\#}$ vs. control group, $^{\#}$, $^{\#\#}$, and $^{\#\#\#}$ indicate $P < 0.05$, $P < 0.01$, and $P < 0.001$, respectively; * vs. IR + FlaA N/C group, *, **, and *** indicate $P < 0.05$, $P < 0.01$, and $P < 0.001$, respectively

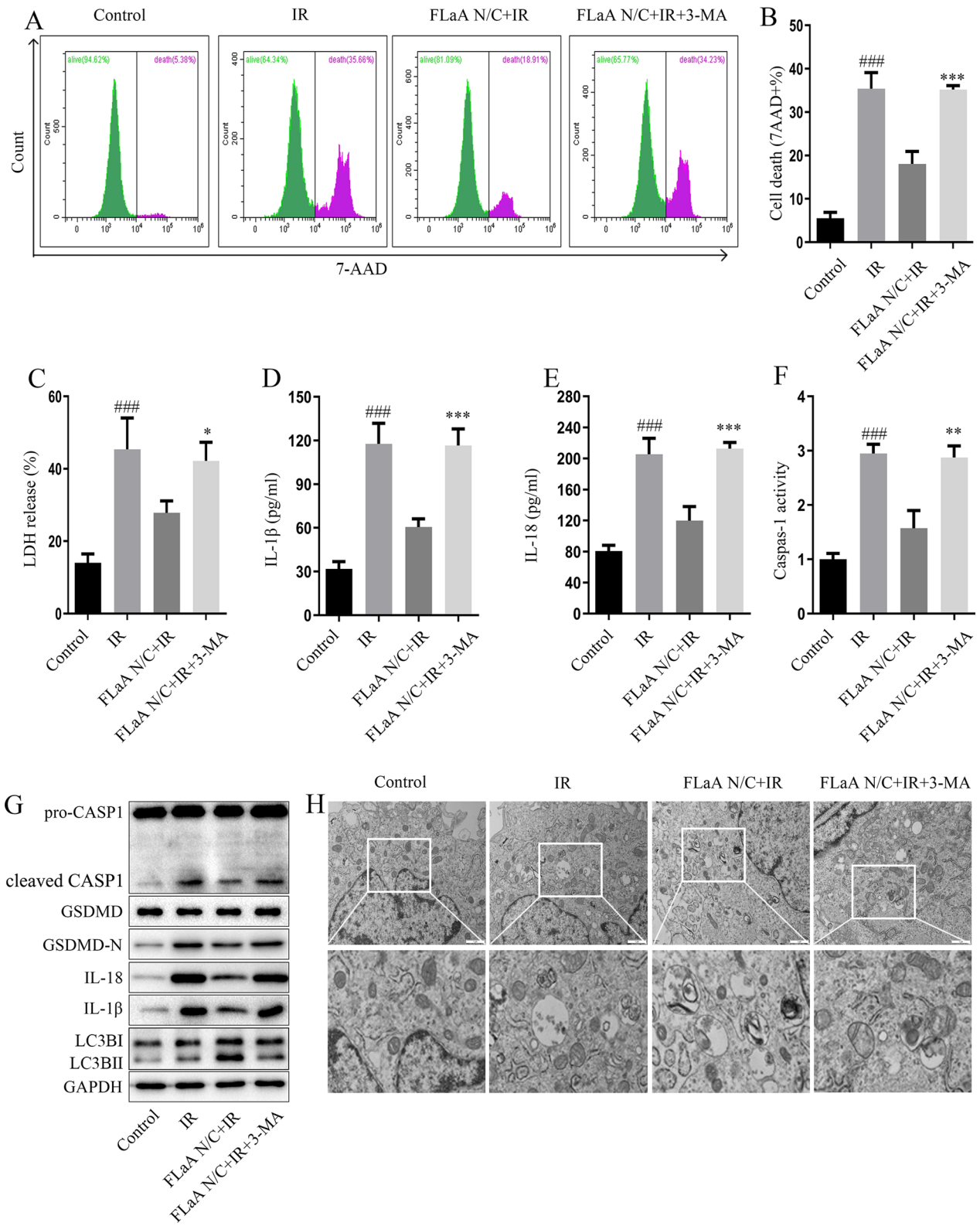

Fig. 8 (See legend on previous page.)

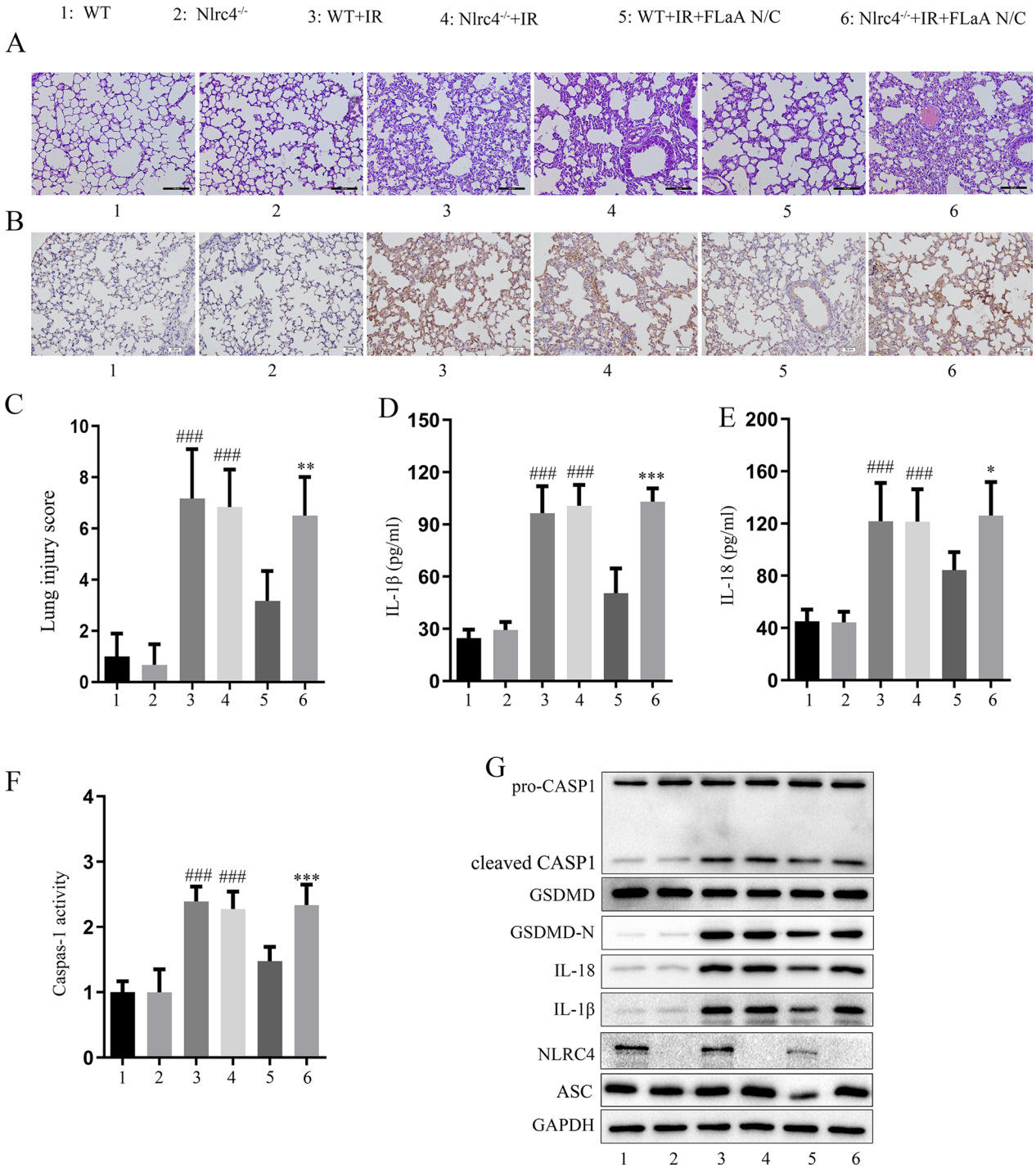

Fig. 9 *Nlrc4* knockout reverses FlaA N/C-induced inhibition of pyroptosis. **a** Representative hematoxylin and eosin (H&E)-stained mouse lung tissue images (scale bars = 100 μm). **b** Representative images of mouse lung tissues stained for GSDMD-N using IHC (scale bars = 50 μm). **c** Lung injury score. **d**, **e** Levels of IL-1β and IL-18 in the serum. **f** Viability of caspase-1 in the lung tissue. **g** Expression of IL-1β, IL-18, caspase-1 p20, GSDMD-N, NLRC4, and ASC in lung tissues was detected using WB. The data are shown as the mean ± SD. $^{\#}$ vs. WT group, $^{\#}$, $^{\#\#}$, and $^{\#\#\#}$ indicate $P < 0.05$, $P < 0.01$, and $P < 0.001$, respectively; * vs. WT + IR + FlaA N/C group, *, **, and *** indicate $P < 0.05$, $P < 0.01$, and $P < 0.001$, respectively

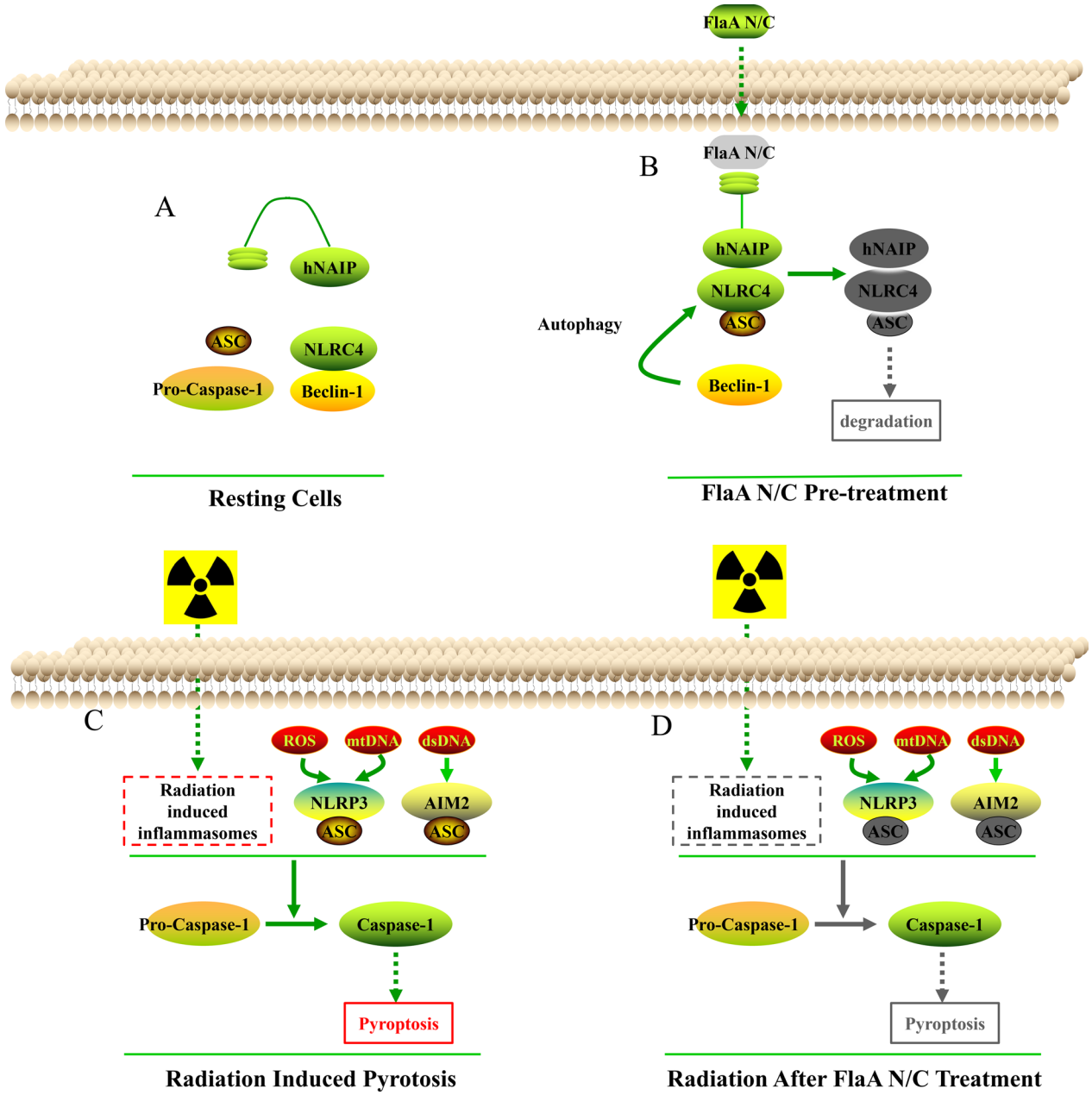

Fig. 10 Diagram of the mechanisms underlying FlaA N/C attenuates RILI. FlaA N/C inhibits radiation-induced pyroptosis by promoting autophagy-mediated degradation of the NAIP/NLRC4/ASC inflammasome. A. In the resting state, Beclin-1 and NLRC4 exist as a complex. B. FlaA N/C entering the cell recruit NLRC4 to form the hNAIP-NLRC4 inflammasome complex, while free Beclin-1 mediates the autophagic degradation of the NAIP-NLRC4 inflammasome, leading to ASC depletion. C. Radiation induces pyroptosis by activating ASC-dependent NLRP3 and AIM2 inflammasomes. D. FlaA N/C treatment mediates the autophagic degradation of the hNAIP-NLRC4 inflammasome, thereby suppressing radiation-induced pyroptosis

applications. However, further investigation of this topic is required.

Abbreviations

3-MA	3-Methyladenine
EdU	5′-Ethynyl-2′-deoxyuridine
AIM2	Apoptosis inhibitor of macrophage 2
ASC	Apoptosis-associated speck-like protein containing a caspase recruitment domain
BALF	Bronchoalveolar lavage fluid
CCK-8	Cell Counting Kit-8
Con	Control
ELISA	Enzyme-linked immunosorbent assay
ΔFLaAN/C	FLaAN/C and D0 domain deletion FLaAN/C
FlaA N/C	Flagellin A with linked C- and N-terminal ends
GSDMD	Gasdermin D

H&E	Hematoxylin and eosin
IF	Immunofluorescence
IHC	Immunohistochemical
IL	Interleukin
IR	Ionizing radiation
KO	Knockout
LDH	Lactate dehydrogenase
LC3	Light chain 3
NAIP	Neuronal apoptosis inhibitory protein
NLRP	NLR family pyrin domain containing
RILI	Radiation-induced lung injury
ROS	Reactive oxygen species
qRT-PCR	Real-time fluorescent quantitative polymerase chain reaction
TEM	Transmission electron microscopy
TNF	Tumor necrosis factor
WB	Western blotting
WT	Wild-type

Supplementary Information

The online version contains supplementary material available at https://doi.org/10.1186/s12967-025-06257-0.

Additional file 1: Fig. S1 In vivo biosafety validation of FlaA N/C. H&E staining images of the major organs except lung (intestine, liver, spleen, kidney and heart) collected from the mice after FlaA N/C treatment (1 mg/kg).

Additional file 2: Fig. S2 FlaA N/C attenuates radiation induced pyroptosis in vivo. Representative hematoxylin and eosin (H&E) stained mouse lung tissue images (scale bars = 100 μm). (B) Representative images of mouse lung tissues stained with GSDMD-N determined by immunohistochemistry (scale bars = 100 μm). (C) The expression of IL-1β, IL-18, and caspase-1 p20 and GSDMD-N in the mouse lung tissues was detected by WB. (D, E) Levels of IL-1β and IL-18 in the mouse serum. # vs. control group, #, ##, and ### indicate $P < 0.05$, $P < 0.01$, and $P < 0.001$, respectively; * vs. IR group, *, **, and *** indicate $P < 0.05$, $P < 0.01$, and $P < 0.001$, respectively.

Additional file 3: Fig. S3 NLRP3 and AIM2 inflammasome mediate radiation-induced pyroptosis. A co-IP assay was used to detect the binding of ASC with NLRC4, AIM2, and NLRP3 in BEAS-2B cells.

Additional file 4: Fig. S4 NLRC4 silencing reversed the FlaA N/C mediated interaction and colocalization of NAIP and ASC. (A) A co-IP assay was used to detect the binding of ASC with NLRC4, and NAIP in BEAS-2B cells. (B) Colocalization of the NAIP and ASC in BEAS-2B cells was detected using fluorescence (scale bars = 10 μm).

Additional file 5: Fig S5 D0 domain deletion reverses the inhibitory effect of FlaA N/C on pyroptosis in vivo. (A, B) Levels of IL-1β and IL-18 in the mouse serum. (C) Viability of caspase-1 in the mouse lung tissue. (D) Representative images of mouse lung tissues stained with GSDMD-N determined by immunohistochemistry (scale bars = 50 μm). (E) Expression of IL-1β, IL-18, caspase-1 p20 and GSDMD-N, and LC3 in mouse lung tissues detected by WB. # vs. control group, #, ##, and ### indicate $P < 0.05$, $P < 0.01$, and $P < 0.001$, respectively; * vs. IR + FlaA N/C group, *, **, and *** indicate $P < 0.05$, $P < 0.01$, and $P < 0.001$, respectively.

Acknowledgements
For their English language editing, we are grateful to Editage (www.editage.cn)

Author contributions
SD, YY, SH, and ZC: data collection and writing, reviewing, and editing original manuscript. XX, TZ, QY, and TL: research materials, software, and methodology. YX, KP, and DW: visualization, validation, supervision, conceptualization, investigation, and writing, reviewing, and editing original manuscript. All authors have read and approved the final manuscript.

Funding
This study was funded by the National Natural Science Foundation of China (Grant numbers 81972977, 82273574, 82273433, and 82203157), Chengdu Medical College United Xindu District People's Hospital Open Subject (Grant numbers 2022LHXD-01 and 2021LHZD-07), Chengdu Medical College United Pidu District People's Hospital Open Subject (Grant number 23LHPDZZD02), Chengdu Medical College United Nanbu People's Hospital Open Subject (Grant number 23LHNBZZD03), Sichuan Medical Association (Grant number Q21004), and Foundation of Sichuan Science and Technology Agency (2021YFG0316).

Availability of data and materials
The data will be made available upon reasonable request.

Declarations

Ethics approval and consent to participate
All animal experiments were approved by The Animal Policy and Welfare Committee of Chengdu Medical College (Approval No: CMC-IACUC-2021024).

Consent for publication
Not applicable.

Competing interests
The authors declare that they have no competing interests.

Author details
[1]School of Clinical Medicine, Chengdu Medical College, Chengdu, Sichuan 610500, People's Republic of China. [2]Clinical Laboratory, The First Affiliated Hospital of Chengdu Medical College, No. 278, Baoguang Road, Chengdu, Sichuan 610500, People's Republic of China. [3]Sichuan Clinical Research Center for Radiation and Therapy, The First Affiliated Hospital of Chengdu Medical College, Chengdu, Sichuan 610500, People's Republic of China. [4]Chengdu Medical College, No. 783, Xindu Road, Chengdu, Sichuan 610500, People's Republic of China.

Received: 20 November 2024 Accepted: 17 February 2025
Published online: 27 February 2025

References

1. Rosic G, Selakovic D, Omarova S. Cancer signaling, CELL/GENE therapy, diagnosis and role of nanobiomaterials. Adv Biol Earth Sci. 2024;9:11–34. https://doi.org/10.62476/abes9s11.
2. Montazersaheb S, Eftekhari A, Shafaroodi A, Tavakoli S, Jafari S, Baran A, et al. Green-synthesized silver nanoparticles from peel extract of pumpkin as a potent radiosensitizer against triple-negative breast cancer (TNBC). Cancer Nanotechnol. 2024;15:47.
3. Feng Y, Yuan P, Guo H, Gu L, Yang Z, Wang J, et al. METTL3 mediates epithelial-mesenchymal transition by modulating FOXO1 mRNA N6 -Methyladenosine-Dependent YTHDF2 binding: a novel mechanism of radiation-induced lung injury. Adv Sci (Weinh). 2023;10: e2204784. https://doi.org/10.1002/advs.202204784.
4. Dasgupta Q, Jiang A, Wen AM, Mannix RJ, Man Y, Hall S, et al. A human lung alveolus-on-a-chip model of acute radiation-induced lung injury. Nat Commun. 2023;14:6506. https://doi.org/10.1038/s41467-023-42171-z.
5. Benveniste MFK, Welsh J, Godoy MC, Betancourt SL, Mawlawi OR, Munden RF. New era of radiotherapy: an update in radiation-induced lung disease. Clin Radiol. 2013;68:e275–90. https://doi.org/10.1016/j.crad.2013.01.013.
6. Wu J, Gou W, Wang Z, Chang H, Li D, Hou W, Liu C. Discovery of the radio-protecting effect of Ecliptae Herba, its constituents and targeting p53-mediated apoptosis in vitro and invivo. Acta Pharm Sin B. 2023;13:1216–30. https://doi.org/10.1016/j.apsb.2022.09.003.
7. Zhang D, Zhong D, Ouyang J, He J, Qi Y, Chen W, et al. Microalgae-based oral microcarriers for gut microbiota homeostasis and intestinal protection in cancer radiotherapy. Nat Commun. 2022;13:1413. https://doi.org/10.1038/s41467-022-28744-4.
8. Liu T, Wu DM, Zhang F, Zhang T, He M, Zhao YY, et al. miR-142a-3p enhances FlaA N/C protection against radiation-mediated intestinal injury by modulating the IRAK1/NF-κB signaling pathway. Int J Radiat Oncol Biol Phys. 2022;112:1256–68. https://doi.org/10.1016/j.ijrobp.2021.12.003.

9. Li L, Deng S, Liu M, Yang M, Li J, Liu T, et al. Novel recombinant protein flagellin A N/C attenuates experimental autoimmune encephalomyelitis by suppressing the ROS/NF-κB/NLRP3 signaling pathway. Front Pharmacol. 2022;14(13): 956402. https://doi.org/10.3389/fphar.2022.956402.
10. Wang J, Zhao J, Ma F, Gong L, Lu Y, Xiao W, et al. One stone, two birds: a peptide-Au(I) infinite coordination supermolecule for the confederate physical and biological radiosensitization in cancer radiation therapy. Small. 2023;19: e2204238. https://doi.org/10.1002/smll.202204238.
11. Hu B, Jin C, Li HB, Tong J, Ouyang X, Cetinbas NM, et al. The DNA-sensing AIM2 inflammasome controls radiation-induced cell death and tissue injury. Science. 2016;354:765–8. https://doi.org/10.1126/science.aaf7532.
12. Li X, Gong Y, Li D, Xiang L, Ou Y, Jiang L, et al. Low-dose radiation therapy promotes radiation pneumonitis by activating NLRP3 inflammasome. Int J Radiat Oncol Biol Phys. 2020;107:804–14. https://doi.org/10.1016/j.ijrobp.2020.02.643.
13. Wang Y, Gao W, Shi X, Ding J, Liu W, He H, et al. Chemotherapy drugs induce pyroptosis through caspase-3 cleavage of a gasdermin. Nature. 2017;547:99–103. https://doi.org/10.1038/nature22393.
14. Toldo S, Abbate A. The role of the NLRP3 inflammasome and pyroptosis in cardiovascular diseases. Nat Rev Cardiol. 2024;21:219–37. https://doi.org/10.1038/s41569-023-00946-3.
15. Zhang Y, Li Z, Hong W, Hsu S, Wang B, Zeng Z, Du S. STING-dependent sensing of self-DNA driving pyroptosis contributes to radiation-induced lung injury. Int J Radiat Oncol Biol Phys. 2023;15(117):928–41. https://doi.org/10.1016/j.ijrobp.2023.05.029.
16. Zhang M, Lan H, Jiang M, Yang M, Chen H, Peng S, et al. NLRP3 inflammasome mediates pyroptosis of alveolar macrophages to induce radiation lung injury. J Hazard Mater. 2024;1(484): 136740. https://doi.org/10.1016/j.jhazmat.2024.136740.
17. Debnath J, Gammoh N, Ryan KM. Autophagy and autophagy-related pathways in cancer. Nat Rev Mol Cell Biol. 2023;24:560–75. https://doi.org/10.1038/s41580-023-00585-z.
18. Zhang G, Du Y, Sun N, Sun Y, Zhang L, Li X, Li X. Ulinastatin enhances autophagy against radiation-induced lung injury in mice. Transl Cancer Res. 2020;9:4162–72. https://doi.org/10.21037/tcr-19-3018.
19. Chen X, Qin W, Wang L, Jin Y, Tu J, Yuan X. Autophagy gene Atg7 regulates the development of radiation-induced skin injury and fibrosis of skin. Skin Res Technol. 2023;29: e13337. https://doi.org/10.1111/srt.13337.
20. Luo N, Zhu W, Li X, Fu M, Zhang Y, Yang F, et al. Defective autophagy of pericytes enhances radiation-induced senescence promoting radiation brain injury. Neuro Oncol. 2024;5(26):2288–304. https://doi.org/10.1093/neuonc/noae153.
21. Liu L, Yi G, Li X, Chen C, Chen K, He H, et al. IL-17A's role in exacerbating radiation-induced lung injury: autophagy impairment via the PP2A-mTOR pathway. Biochim Biophys Acta Mol Cell Res. 2025;1872: 119864. https://doi.org/10.1016/j.bbamcr.2024.119864.
22. Wang L, Cai J, Zhao X, Ma L, Zeng P, Zhou L, et al. Palmitoylation prevents sustained inflammation by limiting NLRP3 inflammasome activation through chaperone-mediated autophagy. Mol Cell. 2023;83:281-297.e10. https://doi.org/10.1016/j.molcel.2022.12.002.
23. Zhu X, Li S, Lin Q, Shao X, Wu J, Zhang W, et al. αKlotho protein has therapeutic activity in contrast-induced acute kidney injury by limiting NLRP3 inflammasome-mediated pyroptosis and promoting autophagy. Pharmacol Res. 2021;167: 105531. https://doi.org/10.1016/j.phrs.2021.105531.
24. Izumi Y, Nakashima T, Masuda T, Shioya S, Fukuhara K, Yamaguchi K, et al. Suplatast tosilate reduces radiation-induced lung injury in mice through suppression of oxidative stress. Free Radic Biol Med. 2019;20(136):52–9. https://doi.org/10.1016/j.freeradbiomed.2019.03.024.
25. Wu X, Ji H, Wang Y, Gu C, Gu W, Hu L, Zhu L. Melatonin alleviates radiation-induced lung injury via regulation of miR-30e/NLRP3 axis. Oxid Med Cell Longev. 2019;10(2019):4087298. https://doi.org/10.1155/2019/4087298.
26. Deng S, Li J, Li L, Lin S, Yang Y, Liu T, et al. Quercetin alleviates lipopolysaccharide-induced acute lung injury by inhibiting ferroptosis via the Sirt1/Nrf2/Gpx4 pathway. Int J Mol Med. 2023;52:118. https://doi.org/10.3892/ijmm.2023.5321.
27. Gurusamy M, Nasseri S, Rampa DR, Feng H, Lee D, Pekcec A, et al. Inhibition of microsomal prostaglandin E synthase-1 ameliorates acute lung injury in mice. J Transl Med. 2021;19:340. https://doi.org/10.1186/s12967-021-03016-9.
28. Lightfield KL, Persson J, Brubaker SW, Witte CE, von Moltke J, Dunipace EA, et al. Critical function for Naip5 in inflammasome activation by a conserved carboxy-terminal domain of flagellin. Nat Immunol. 2008;9:1171–8. https://doi.org/10.1038/ni.1646.
29. Guan D, Mi J, Chen X, Wu Y, Yao Y, Wang L, et al. Lung endothelial cell-targeted peptide-guided bFGF promotes the regeneration after radiation induced lung injury. Biomaterials. 2018;184:10–9. https://doi.org/10.1016/j.biomaterials.2018.08.061.
30. Zhang W, Wu Q, Zhang X, Qin Y, Gao L, Hu S, et al. NLRP3 promotes radiation-induced brain injury by regulating microglial pyroptosis. Neuropathol Appl Neurobiol. 2024;50: e12992. https://doi.org/10.1111/nan.12992.
31. Wei J, Zhao Q, Zhang Y, Shi W, Wang H, Zheng Z, et al. Sulforaphane-mediated Nrf2 activation prevents radiation-induced skin injury through inhibiting the oxidative-stress-activated DNA damage and NLRP3 inflammasome. Antioxidants (Basel). 2021;10:1850. https://doi.org/10.3390/antiox10111850.
32. Han C, Godfrey V, Liu Z, Han Y, Liu L, Peng H, et al. The AIM2 and NLRP3 inflammasomes trigger IL-1-mediated antitumor effects during radiation. Sci Immunol. 2021;6:eabc6998. https://doi.org/10.1126/sciimmunol.abc6998.
33. Jiang H, Xie Y, Lu J, Li H, Zeng K, Hu Z, et al. Pristimerin suppresses AIM2 inflammasome by modulating AIM2-PYCARD/ASC stability via selective autophagy to alleviate tendinopathy. Autophagy. 2024;20:76–93. https://doi.org/10.1080/15548627.2023.2249392.
34. Sun Q, Fan J, Billiar TR, Scott MJ. Inflammasome and autophagy regulation—a two-way street. Mol Med. 2017;23:188–95. https://doi.org/10.2119/molmed.2017.00077.
35. Di Q, Zhao X, Tang H, Li X, Xiao Y, Wu H, et al. USP22 suppresses the NLRP3 inflammasome by degrading NLRP3 via ATG5-dependent autophagy. Autophagy. 2023;19:873–85. https://doi.org/10.1080/15548627.2022.2107314.
36. Jounai N, Kobiyama K, Shiina M, Ogata K, Ishii KJ, Takeshita F. NLRP4 negatively regulates autophagic processes through an association with beclin1. J Immunol. 2011;186:1646–55. https://doi.org/10.4049/jimmunol.1001654.
37. Xu C, Wang L, Fozouni P, Evjen G, Chandra V, Jiang J, et al. SIRT1 is downregulated by autophagy in senescence and ageing. Nat Cell Biol. 2020;22:1170–9. https://doi.org/10.1038/s41556-020-00579-5.

Publisher's Note